Materials Research Proceedings 41 (2024) 2252-2260 https://doi.org/10.21741/9781644903131-248

# Investigations on the temperature and strain rate dependent behavior of a reinforced thermoplastic: application in hot incremental forming

FADDOULD Josephine[1,2,a], RAHME Pierre[3,b], GUINES Dominique[1,c*] and LEOTOING Lionel[1,d*]

[1]Univ Rennes, INSA Rennes, LGCGM (Laboratoire de Génie Civil et Génie Mécanique), Rennes, France

[2]Faculty of Engineering, Mechanical Engineering Department, Lebanese University, Lebanon

[3]Department of Industrial and Mechanical Engineering, Lebanese American University, Lebanon

[a]josephine.faddoul@insa-rennes.fr, [b]pierre.rahme@lau.edu.lb, [c]dominique.guines@insa-rennes.fr, [d]lionel.leotoing@insa-rennes.fr

**Keywords:** Reinforced Thermoplastic, Thermo-Viscoplasticity, FE Modeling, Mechanical Characterization

**Abstract.** This study focuses on characterizing the thermo-viscoplastic behavior of a glass fiber reinforced polypropylene through an advanced characterization technique. Based on a preliminary work addressing a mechanical characterization from conventional uniaxial tests, the proposed rheological model is calibrated using the database of in-plane equi-biaxial tensile tests on a dedicated cruciform specimen geometry from room temperature up to *140°C*. The Finite Element Model Update (FEMU) method is employed for parameter calibration. A comparative analysis with the model calibrated from prior uniaxial tests is conducted through finite element simulations of a forming process. This investigation includes a parametric study to objectively assess the impact of the behavior law on forming force and final profile. This parametric study has direct implications for the simulation of an original forming process. The ability to identify the differences in forming outcomes based on different behavior laws enhances the predictive accuracy of the simulations. This ensures that the chosen behavior law aligns closely with the real behavior of the material during forming.

## Introduction

Fiber reinforced thermoplastics, known for their good mechanical properties and recyclability, are extensively applied in engineering applications. Finite element (FE) simulations of the forming processes are essential to avoid trials and errors but require accurate representation of the material behavior under real conditions: multiaxial loading with large deformations, varying temperatures, and strain rates [1].

In-plane biaxial tensile tests using flat cruciform specimens are promising for achieving biaxial loading states. This frictionless technique allows direct application of loads along the two perpendicular arms of the specimen, offering versatility with multiple strain paths, from uniaxial to equi-biaxial stretching. Depending on the requirements and objectives of the mechanical characterization, the shape of the cruciform specimen can be modified and adjusted. This technique is commonly used to characterize metals. For instance, Liu et al. [2] proposed an optimized specimen design to investigate the hardening behavior of metallic sheets under conditions involving significant strains. Recently, some studies have explored the applicability of this technique to fiber reinforced polymers. Smits et al. [3] conducted a comparative study to investigate the influence of different specimen geometries on the biaxial failure strain of glass fiber reinforced epoxy composites. Their work aimed to identify a suitable specimen geometry for

conducting biaxial tests on fiber reinforced composites providing valuable insights into the testing methodology for these materials.

This study focuses on characterizing the thermo-viscoplastic behavior of a glass fiber reinforced polypropylene using in-plane biaxial tensile tests conducted on a dedicated cruciform specimen. The material parameters for the modified G'Sell and Jonas model proposed in a prior study [4] are identified relying on the biaxial experimental results. The calibrated model is then used to simulate a hot incremental sheet forming process. The forming outcomes are compared with simulations using material parameters identified from conventional uniaxial tensile tests.

## Material and experimental setup

The material used in this work is a *40%* discontinuous long glass fiber reinforced polypropylene thermoplastic. Injected molded plates of *510×300×2 mm*$^3$ are supplied by SABIC (Stamax, 40YM240 [5]). The cruciform specimen proposed by Liu et al. [2] is considered in this study. It was proven that this shape can guarantee large equivalent plastic strains in the central zone under biaxial tensile loadings. The design and dimensions of the specimen are presented in Fig. 1. The samples are extracted by water-jet cutting. From a *2mm* initial thickness, a thinning of the central zone is achieved by milling (down to a reduced thickness of *0.625 mm*) to ensure failure in this zone.

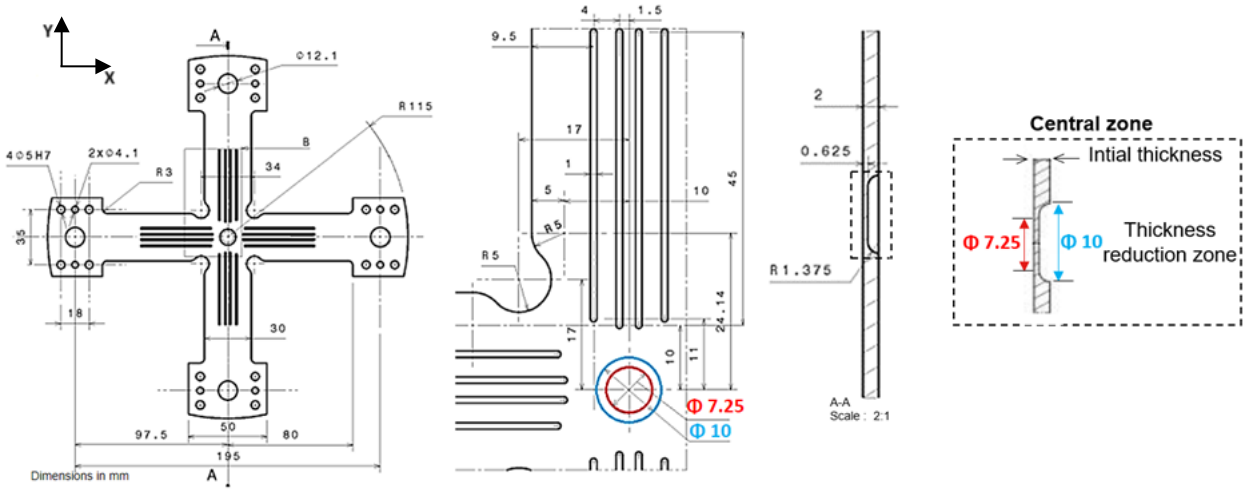


*Figure 1: Geometry of cruciform specimen designed by Liu et al. [2]*

A specialized quasi-static/dynamic biaxial tensile device is used in this work to perform the in-plane biaxial tensile tests. Fig. 2 shows the experimental apparatus for a test performed at a high temperature.

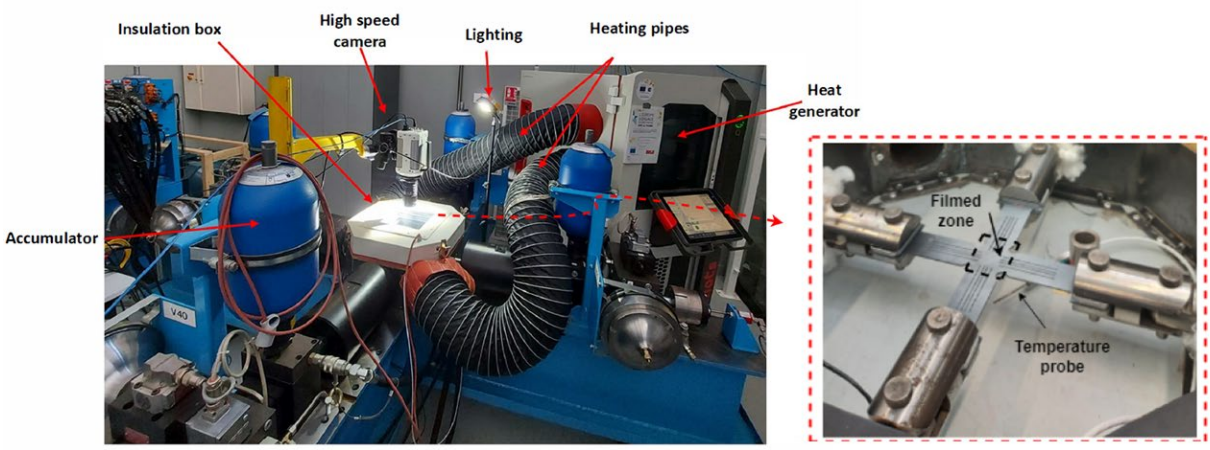


*Figure 2: Experimental apparatus of the in-plane biaxial tensile test*

Two load sensors, which connect the grip system and the sliding bar, are placed to measure the forces along both perpendicular directions X and Y. For tests conducted at elevated temperatures, a heating system is added to the apparatus. It comprises an airflow generator and an insulated box. A high-speed camera (PHOTRON FASTCAM NOVA S9) is positioned along the central vertical axis of the biaxial bench to capture sequential images of the specimen during the test. The in-plane strain fields are then measured using the Digital Image Correlation DIC technique. The images are post-processed using the software "GOM Correlate".

**Experimental results and discussion**

The temporal evolution of the biaxial forces ($F_X$ and $F_Y$) as well as the in-plane principal $\varepsilon_1$, $\varepsilon_2$ and equivalent $\bar{\varepsilon}$ strains, are mainly concerned. Fig. 3 shows the force and strain curves resulting from the in-plane biaxial tensile test at room temperature (*RT*) and quasi-static velocity of *0.1mm/s*. As shown in the figure, maximum forces of $F_{Xf} = 1400\ N$ and $F_{Yf} = 1100\ N$ are obtained at failure (the subscript *f* designates the value at failure). The difference between both curves is mainly attributed to the material anisotropy. The influence is also visible on the curves showing the temporal evolution of $\varepsilon_1$ and $\varepsilon_2$. The maximum level of strain reached just before failure is $\varepsilon_{1f} = 1\%$ and $\varepsilon_{f2} = 2\%$, respectively. $\bar{\varepsilon}$ is found to have a maximum value of $\bar{\varepsilon}_f = 3.2\%$ at failure.

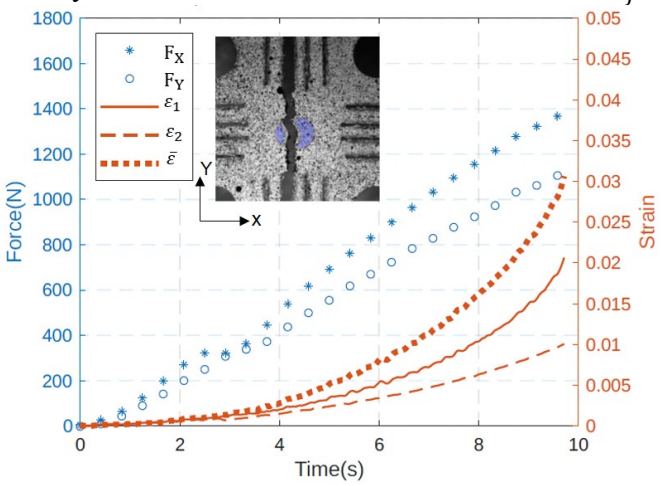


*Figure 3: In-plane biaxial tensile test at RT and V=0.1mm/s*

Consistent patterns in the evolution of both forces and strains were observed across all temperature conditions, up to 140°C. It was noted that the maximum force decreases in approximately a linear trend with temperature increase, whereas the maximum equivalent strain increases exponentially. The values are summarized in Table 1. $F_f$ is the average of $F_{Xf}$ and $F_{Yf}$

measured along both directions just before failure. The temperature effect on the maximum equivalent strain is clearly pronounced at the highest temperatures. A *5°C* gap causes a significant increase in the maximum equivalent strain level, i.e. $\bar{\varepsilon}_f$ increases by *50%* when the temperature increases from *135* to *140°C*.

*Table 1: Temperature sensitivity of maximum biaxial force and equivalent strain*

| *T (°C)* | RT | 70 | 100 | 120 | 130 | 135 | 140 |
|---|---|---|---|---|---|---|---|
| $\bar{\varepsilon}_f$*(%)* | 3.1 | 4.6 | 5.6 | 15.8 | 17 | 22 | 33 |
| $F_f$*(N)* | 1140 | 833 | 654 | 364 | 314 | 200 | 185 |

**Thermo-viscoplastic rheological behavior model**

The phenomenological constitutive law of G'Sell and Jonas (1979, 1983) [6,7] is selected to model the behavior of the studied material. This model is considered as an important contribution to understanding the plastic behavior of polymers. It describes the uniaxial stress-strain relation in dependence of strain and strain rate. The model is also capable of representing the hardening of the material after yielding. Several studies relied on this law to predict the stress-strain response of thermoplastics as well as fiber reinforced thermoplastics. For instance, in the study of Schossig et al. [8], the strain-rate-dependent behavior of glass fiber reinforced polypropylene and polybutene 1 was empirically examined and modeled using G'Sell and Jonas formulation.

In this work, the model is presented through one-dimensional elasto-viscoplastic formulation (Eq. 1). The modification of the constitutive equation was proposed in a previous work [4] for a better description of the observed experimental behavior. Additionally, the effect of the temperature is incorporated in the model by performing a temperature sensitivity analysis for the material parameters and expressing them as a function of temperature.

$$\begin{cases} \bar{\sigma}(\bar{\varepsilon}\,,\,\dot{\bar{\varepsilon}}\,,T) = E\,(\dot{\bar{\varepsilon}},T).\bar{\varepsilon} & for\ \bar{\sigma} < \sigma_y \\ \bar{\sigma}(\bar{\varepsilon}\,,\,\dot{\bar{\varepsilon}}\,,T) = \sigma_y(\dot{\bar{\varepsilon}}\,,T) + \mathrm{K(T)}.\ \left(1 - \exp\left(-\mathrm{W}(T)\bar{\varepsilon}_p\right)\right).\dot{\bar{\varepsilon}}^m & for\quad \bar{\sigma} > \sigma_y \end{cases} \tag{1}$$

$\bar{\sigma}$ is the flow stress, $\bar{\varepsilon}$ and $\bar{\varepsilon}_p$ are the total and plastic equivalent strains, respectively. $\dot{\bar{\varepsilon}}$ and *T* refer to the equivalent strain rate and the temperature, respectively. *K* (scaling factor), and *W* are material parameters. *m* represents the strain rate sensitivity. *E* and $\sigma_y$ are the Young's modulus and the yield stress, respectively.

Based on the stress-strain curves determined form the uniaxial tensile tests [4], the formulations of *m* and *E* are found as stated in Eq. 2 and Eq. 3, respectively.

$$m = \left.\frac{\partial \ln\left(\bar{\sigma}\left(\bar{\varepsilon}\,,\dot{\bar{\varepsilon}}\,,T\right) - \sigma_y\right)}{\partial ln\,\dot{\bar{\varepsilon}}}\right|_{\bar{\varepsilon}_p,T} \tag{2}$$

$$\mathrm{E}(\dot{\bar{\varepsilon}}\,,T) = E_0(\mathrm{T}).\dot{\bar{\varepsilon}}^m = E_1.exp\left(A_E\left(\frac{1}{T} - \frac{1}{T_g}\right)\right).\dot{\bar{\varepsilon}}^m \tag{3}$$

Where $E_1$ and $A_E$ are material constants and $T_g$ is the glass transition temperature (*-10°C*).

The proposed model was coupled with Hill 48 plasticity criterion to account for anisotropy [4]. The anisotropic parameters were calibrated based on uniaxial tensile tests for different material orientations.

**FE model of the in-plane biaxial test**

The FE model, implemented in Abaqus software (implicit solver), is optimized for computational efficiency by modeling only one-quarter of the specimen, taking advantage of symmetry considerations (see Fig. 4).

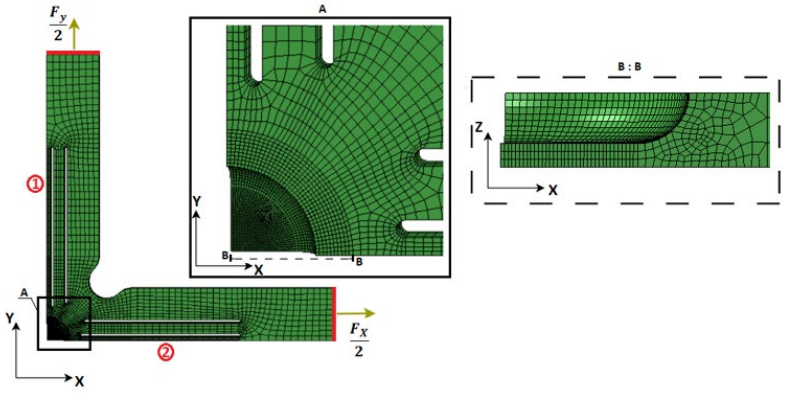


*Figure 4: FE model of the cruciform specimen*

Symmetry conditions are imposed on sides 1 and 2, and the temporal evolution of forces ($F_X/2$ and $F_Y/2$) obtained experimentally is applied along both perpendicular directions. Applying half of the experimental force reproduces the experimental conditions. The 3D mesh of the cruciform specimen is built with 8-nodes brick elements (C3D8R), with a refined element size of *0.1 mm* and three elements arranged along the thickness direction in the central zone, focusing on the in-plane biaxial tensile state.

**Calibration of material parameters**

For mechanical characterization through uniaxial tensile tests, stresses can be directly computed. In contrast, for in-plane biaxial tests with cruciform specimens, direct calculation of stresses and strains is not available. Consequently, based on full-field measurements, an inverse analysis procedure (Finite Element Model Update) becomes necessary for parameter identification. This method involves minimizing the gap between finite element simulation outputs and experimental observations by optimizing material parameters. The SIMPLEX algorithm is employed for the optimization. The temporal evolution of the experimental equivalent strain, from Digital Image Correlation DIC method, and averaged on the central zone of the specimen, is then compared with the simulated equivalent strain. The cost function $Q$ can be calculated (Eq. 4).

$$Q = \sqrt{\frac{\frac{1}{n}\sum_i^n\left(\bar{\varepsilon}_{exp}\,(t_i)-\bar{\varepsilon}_{sim}\,(t_i)\right)^2}{\sum_i^n(\bar{\varepsilon}_{exp}\,(t_i))^2}} \tag{4}$$

Where the simulated and experimental equivalent strains $\bar{\varepsilon}_{sim}$ and $\bar{\varepsilon}_{exp}$ are calculated in the same manner using Eq. 5.

$$\bar{\varepsilon} = \frac{1}{3}(\sqrt{2[(\varepsilon_1-\varepsilon_2)^2+(\varepsilon_2-\varepsilon_3)^2+(\varepsilon_3-\varepsilon_1)^2]} \tag{5}$$

In this equation $\varepsilon_3$ is the out of plane principal strain calculated based on the volume conservation.

In this calibration strategy, the parameters $K$, $\sigma_y$, and $W$ are iteratively adjusted for a better fit with the experimental strain results. The optimized variables are listed in Table 2. The values of

the cost function $Q$ for each parameter set (determined at a specific temperature) show that at the end of the optimization procedure, the model's predictions closely match the experimental observations. For example, at the end of the optimization procedure at T=135°C, the prediction deviates from the experimental data by approximately 5% which is reasonably good.
A temperature sensitivity analysis shows a linear decrease of these parameters as temperature increases.
$E$ and $m$ are excluded from the optimization, based on their prior identification from uniaxial tensile tests [4]. The sensitivity of $E$ to temperature and strain rate is expressed by the physical formulation presented in Eq. 3 with $E_1=12255MPa$ and $A_E=915$. $m$ is assumed to be constant ($m=0.07$) because of the negligible temperature effect on the strain rate sensitivity observed at high temperatures.

*Table 2: Identified parameters based on the experimental equi-biaxial tensile tests*

| $T(°C)$ | $K\ (MPa)$ | $\sigma_y(MPa)$ | $W\ (/)$ | $Q\ (\%)$ |
|---|---|---|---|---|
| 20 | 78.9 | 25 | 134.4 | 5.2 |
| 70 | 36.2 | 29.3 | 117.9 | 7.6 |
| 100 | 30.3 | 23.9 | 72.8 | 6.6 |
| 120 | 24.3 | 10.4 | 44 | 2.6 |
| 130 | 22.5 | 8.9 | 28.75 | 6.7 |
| 135 | 19.9 | 5.6 | 11.2 | 5.2 |
| 140 | 17.5 | 6 | 7 | 2.5 |

FE simulations of the in-plane biaxial tensile tests are performed using the generalized formulation of the model. A well description of the temporal principal and equivalent strains evolution is observed for the tested temperature conditions. Fig. 5 presents the results obtained from the simulation at $T=135°C$ and a quasi-static velocity. The correlation of the simulated in-plane principal strains $\varepsilon_{sim1}$ and $\varepsilon_{sim2}$ is relatively acceptable, even though these parameters are not directly targeted in the cost function.

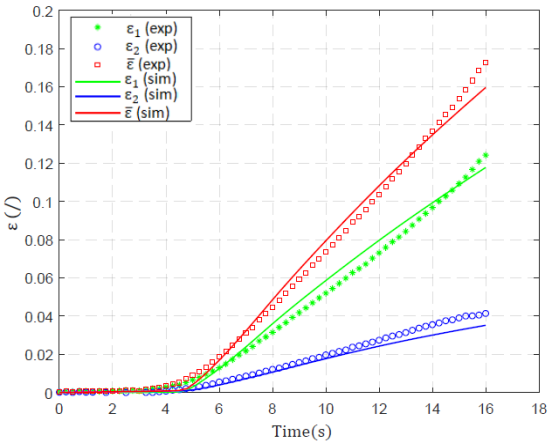


*Figure 5: Comparison of experimental and numerical strain curves at T=135°C*

**Finite element modeling of Incremental Sheet Forming**
Based on the FE modeling of the Incremental Sheet Forming (ISF) process, a parametric study is proposed to investigate the impact of parameters like temperature and behavior law on forming forces and final shape of the part. The FE model is created using ABAQUS software (implicit solver), based on common assumptions from the literature [9]. These assumptions include the use

of shell elements and clamped sheet edges as boundary conditions. To simplify and reduce computation time, the study is conducted on a quarter of the model (see Fig. 6). The "stepped" trajectory shown in Fig. 7 is imposed on the tool. For each cycle, the tool maintains a maximum axial or radial depth increment of 1mm.

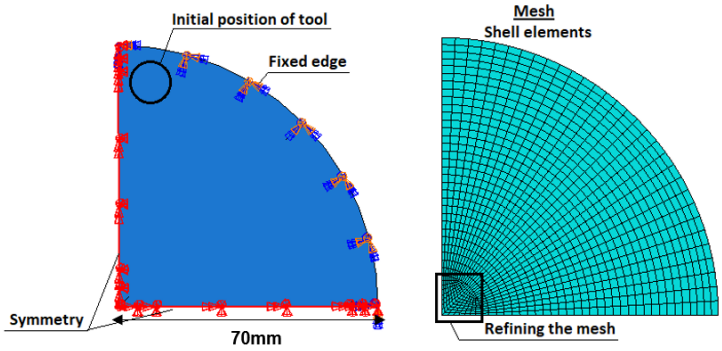


*Figure 6: Representation of the FE model*

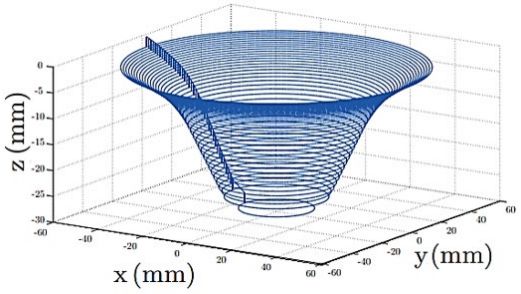


*Figure 7: Tool trajectory with successive circular contours*

Fig. 8 illustrates the effect of the material behavior law on the tool axial force. At *T=120°C*, the difference between the simulated maximum axial force using the law identified from uniaxial tests and the one from in-plane biaxial tests is close to *11%*. This difference increases to *21%* at *T=130°C*, and remains stable for *T=140°C*. The results highlight the clear sensitivity of the forming force on the method to identify the parameters of the material law, which becomes more pronounced at higher temperatures. In contrast, the behavior law has a negligible impact on the simulated final shape for all the tested temperatures, as depicted in Fig. 9. For a better visualization of temperature's effect, the simulation results obtained using the behavior law calibrated from the biaxial database at different temperatures are shown in Fig. 10. Obviously, as temperature increases, the maximum axial force level at the end of forming decreases down to the lowest value of approximately *200N*. On the other hand, the final formed shape of the plate is not affected by the temperature.

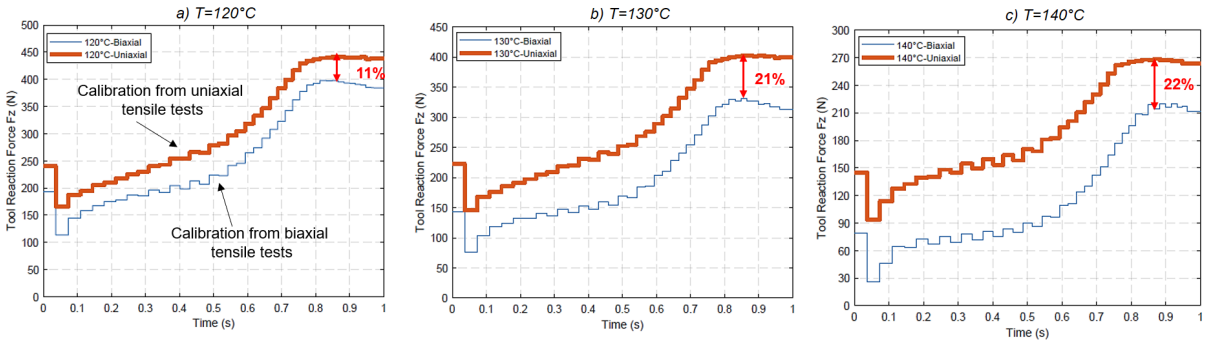


*Figure 8: Effect of behavior law on the tool reaction forces Fz for different test temperatures*

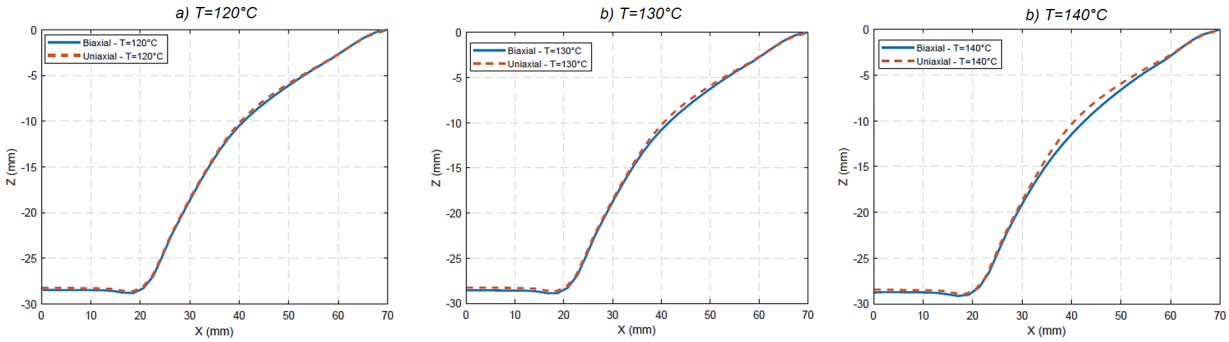


*Figure 9: Effect of behavior law on the profile for different test temperatures*

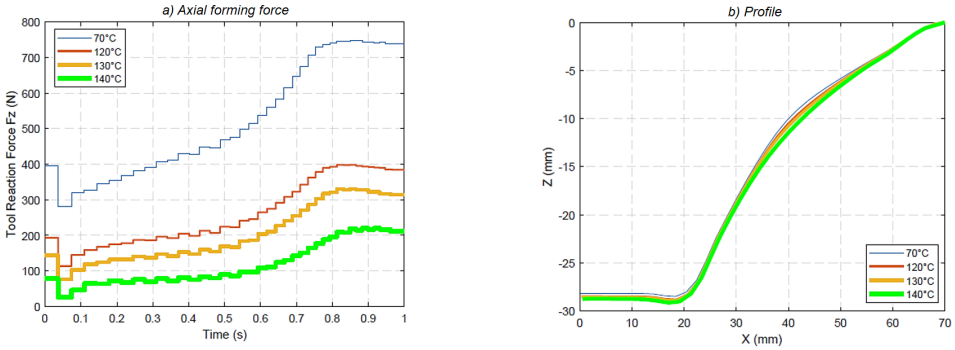


*Figure 10: Effect of temperature on the tool reaction force and final profile*

## Conclusion

In this work, the modified thermo-viscoplastic G'Sell and Jonas model is calibrated according to in-plane biaxial tensile tests on a dedicated cruciform specimen. The purpose of this new identification strategy is to propose a material characterization procedure based on a biaxial strain state close to the one encountered in forming processes. The effect of the identification strategy is evaluated thanks to the FE simulation of the hot incremental forming process of a truncated cone. A parametric study indicates that the simulated forming forces are significantly influenced by temperature and the choice of the rheological law i.e. calibration strategy for model parameters. However, these factors do not impact the simulated profile of the truncated cone. For future work, a heat assisted incremental forming process will be conducted experimentally, providing a basis for validation of the numerical predictive model. This will allow for a careful assessment of the degree of agreement between experimental and simulated results issued from the two different material characterization techniques.

## References

[1] T. Meinders, Emin Semih Perdahcıoğlu, M. van Riel, and H.H. Wisselink, "Numerical modeling of advanced materials," *International Journal of Machine Tools & Manufacture*, 48 (2008) 485–498 https://doi.org/10.1016/j.ijmachtools.2007.08.005

[2] W. Liu, D. Guines, L. Leotoing, and E. Ragneau, "Identification of sheet metal hardening for large strains with an in-plane biaxial tensile test and a dedicated cross specimen," *International Journal of Mechanical Sciences*, 101–102 (2015) 387–398. https://doi.org/10.1016/j.ijmecsci.2015.08.022

[3] A. Smits, D. Van Hemelrijck, T. P. Philippidis, and A. Cardon, 'Design of a cruciform specimen for biaxial testing of fibre reinforced composite laminates', *Composites science and technology*, 66 (2006) 964–975. https://doi.org/10.1016/j.compscitech.2005.08.011

[4] J. Faddoul, P. Rahme, D. Guines, and L. Leotoing, "Thermo-visco mechanical behavior of glass fiber reinforced thermoplastic composite," *Journal of Composite Materials*, 57 (2023) 3741–3754. https://doi.org/10.1177/00219983231192147

[5] "StamaxTM," SABIC, https://www.sabic.com/en/products/polymers/polypropylene-pp/stamax (accessed Feb. 4, 2024).

[6] C. G'Sell and J. J. Jonas, "Determination of the plastic behaviour of solid polymers at constant true strain rate," *Journal of Materials Science*, 14 (1979) 583–591. https://doi.org/ 10.1007/bf00772717

[7] C. G'sell, N. A. Aly-Helal, and J. J. Jonas, 'Effect of stress triaxiality on neck propagation during the tensile stretching of solid polymers', Journal of Materials Science, 18 (1983) 1731–1742. https://doi.org/10.1007/BF00542069

[8] M. Schoßig, C. Bierögel, W. Grellmann, and T. Mecklenburg, 'Mechanical behavior of glass-fiber reinforced thermoplastic materials under high strain rates', *Polymer testing*, 27 (2008) 893–900. https://doi.org/10.1016/j.polymertesting.2008.07.006.

[9] J. Belchior, D. Guines, L. Leotoing, and E. Ragneau, 'Force prediction for correction of robot tool path in single point incremental forming', *Key Engineering Materials*, 554 (2013) 1282–1289. https://doi.org/10.4028/www.scientific.net/kem.554-557.1282